Supplementary Information for：

Ultrahigh voltage direct current quasi-tribovoltaic nanogenerator by switchable tribo-bias induction and deposited charge extraction

*Xuemei Zhang[a], Dahu Ren[a], Huiyuan Wu[a], Jian Wang[a], Xiaochuan Li[a], Huake Yang[a], Qianying Li[a], Qianxi Yang[a], Jinrong Zhu[a], and Yi Xi[a]**

[a] Chongqing Key Laboratory of Soft Condensed Matter Physics and Smart Materials, Department of Applied Physics, Analytical and Testing Center, Chongqing University, Chongqing 400044, P. R. China;

* Corresponding authors at: yxi6@cqu.edu.cn (Yi Xi)

Content

Supplementary Figures

Supplementary Tables

Supplementary Videos

Supplementary Figures

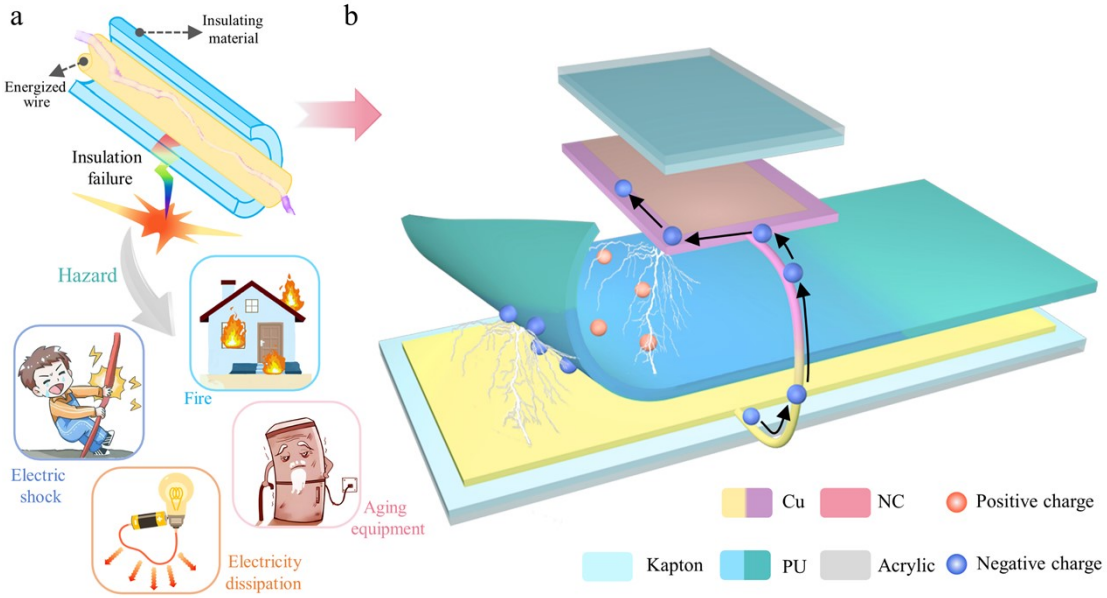

Fig. S1 Hazards and utilization of insulating materials with insulation failure. (a) Schematic diagram of insulation failure. (b) Conceptual diagram of electron group trajectories in I-Q-TVNG based on the insulation failure of charge deposition material.

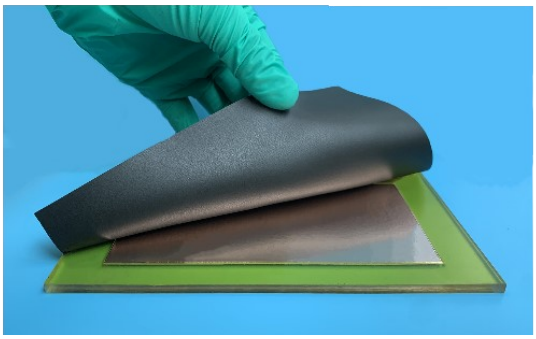

Fig. S2 Photograph of the stator within the sliding type I-Q-TVNG.

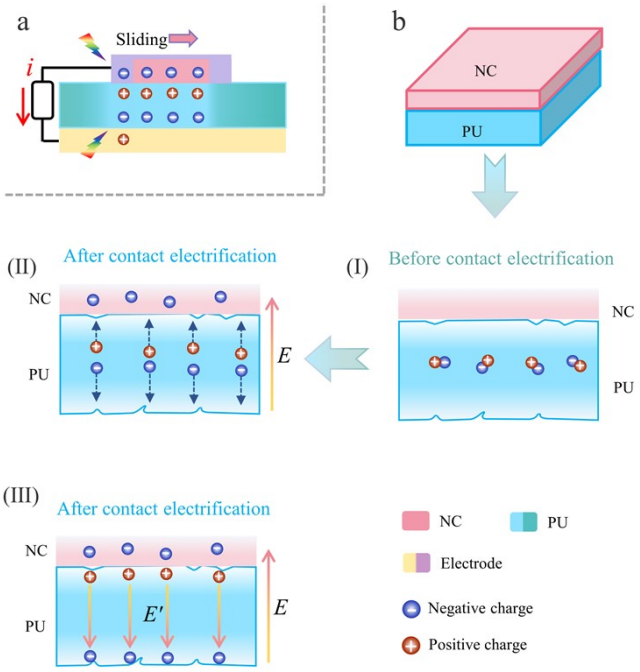

Fig. S3 The formation and effect of tribo-bias in I-Q-TVNG. (a) Structure diagram of I-Q-TVNG. (b) The electric filed effect in the interface of NC and PU. The insert of (I) is the charge distribution inner the PU before contact electrification. The inserts of (II) is the charge enter shifting process after contact electrification, with a tribo-bias (*E*). The inserts of (III) is the forming of build-in electric filed (*E'*).

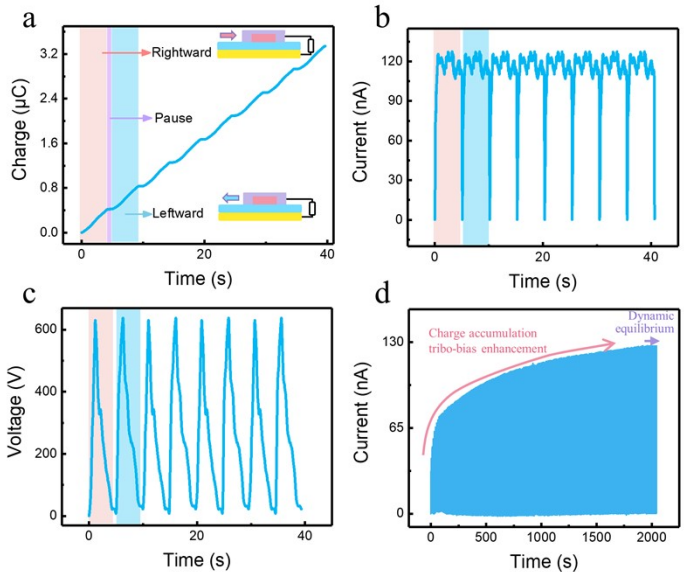

Fig. S4 Output performance of I-Q-TVNG with a slider consisted of NC and Cu electrode. Output charge (a), current (b), and voltage (c) of the sliding-type device during reciprocating motion (forward-pause-backward). (d) Short-circuit current versus time from initial state to steady state.

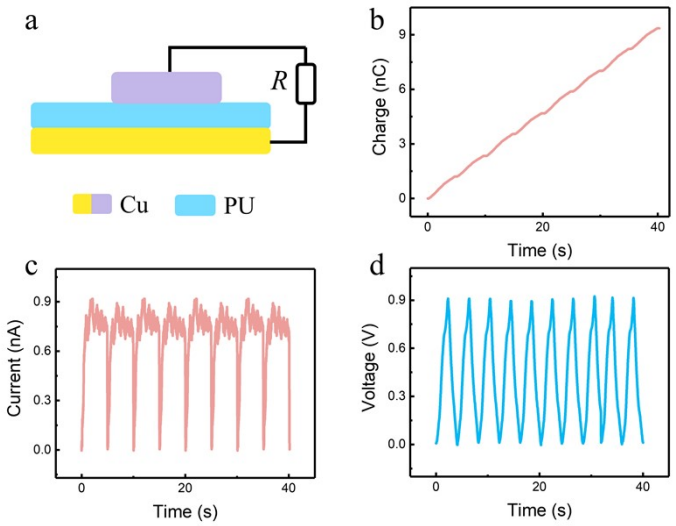

Fig. S5 Output performance of I-Q-TVNG with only Cu electrode as the slider. Output charge (a), current (b), and voltage (c) of the device during reciprocating motion.

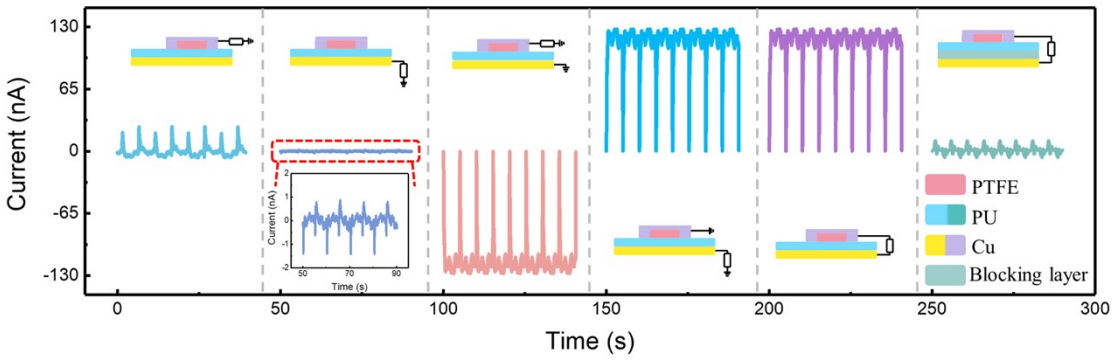

Fig. S6 Output current curve under six working circumstances.

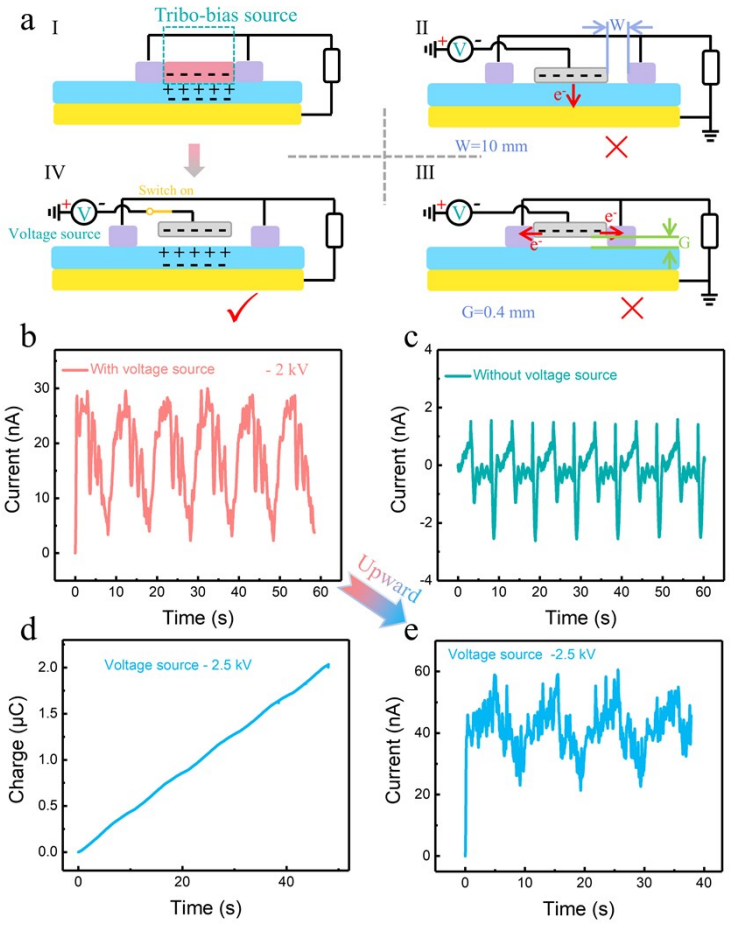

Fig. S7 Output performance of the I-Q-TVNG with a constant voltage source. (a) Location selection of the constant voltage source. (b) Output charge of the device under induced voltage of -2 kV. (c) Output charge of the device without constant voltage source. Output charge (d) and current (e) of the device under voltage of -2.5 kV.

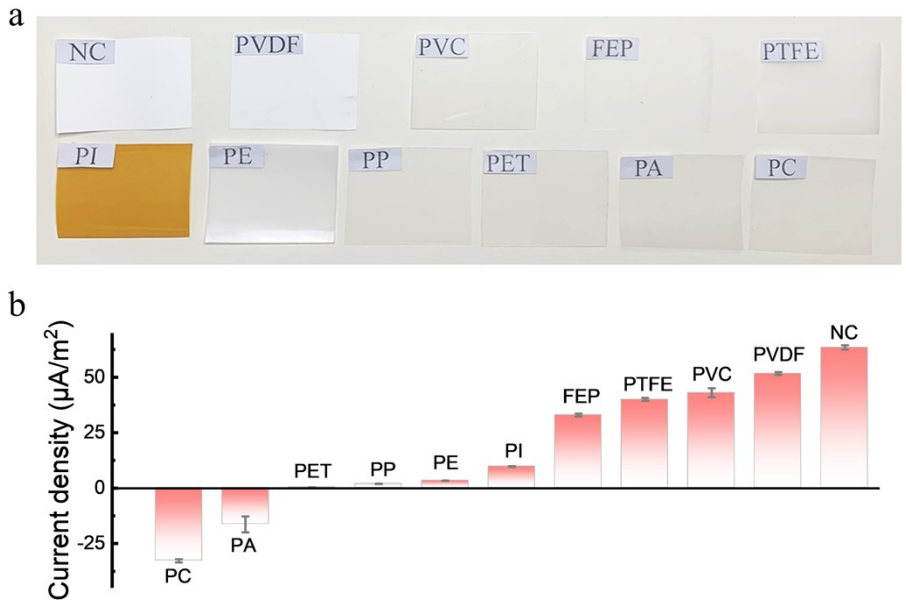

Fig. S8 Selection and evidence of tribo-bias source material. (a) Optical image of common triboelectric materials as the tribo-bias source material in I-Q-TVNG. (b) Current density of I-Q-TVNG with different the tribo-bias source materials.

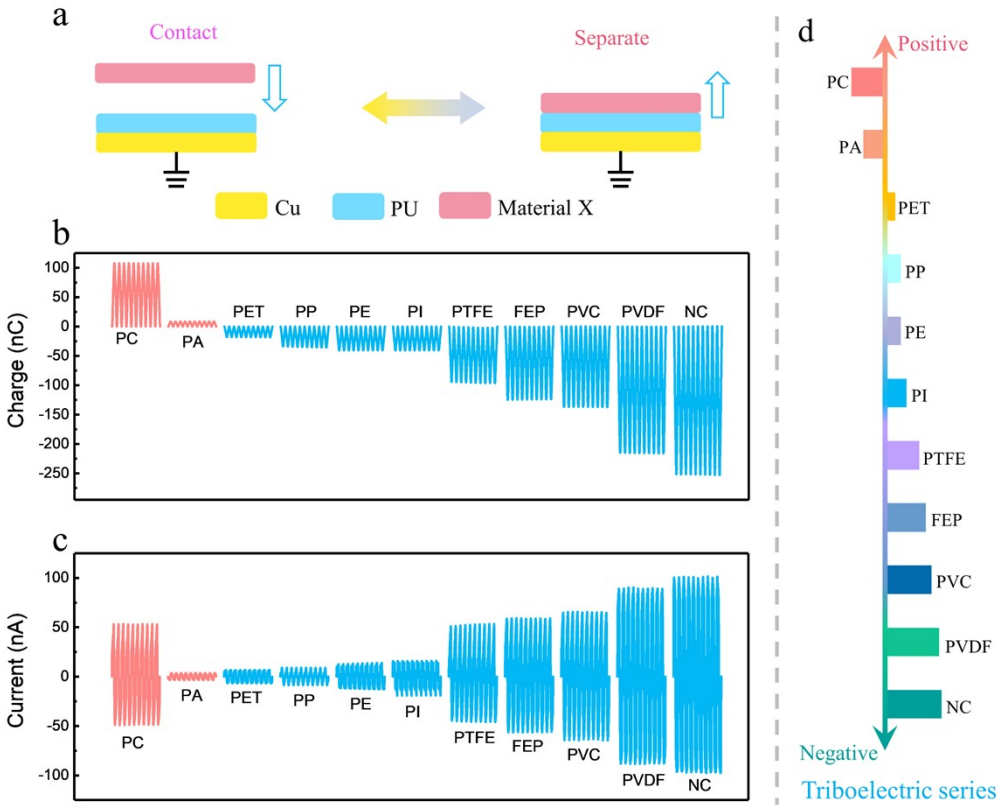

Fig. S9 Output performance of contact-separation AC-TENG with different contact materials. (a) Schematic diagram of the contact-separation TENG. Output charge (b) and (c) current of AC-TENG with different contact materials. (d) The quantified triboelectric series.

Fig. S10 Optical image of common triboelectric materials as the charge deposition materials in I-Q-TVNG.

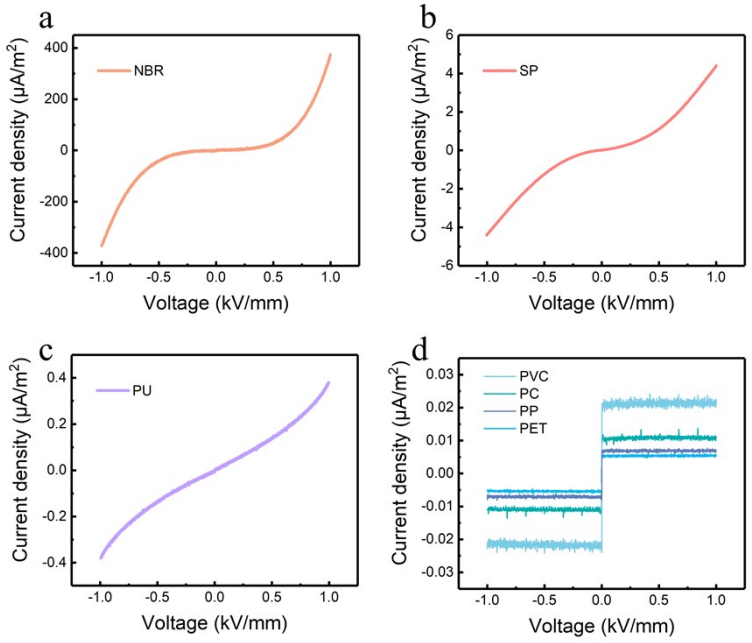

Fig. S11 Leakage current density of seven fixed charge deposition materials. Leakage current density of seven fixed charge deposition materials, NBR (a), SP (b), PU (c), and PC, PVC, PET, PP (d).

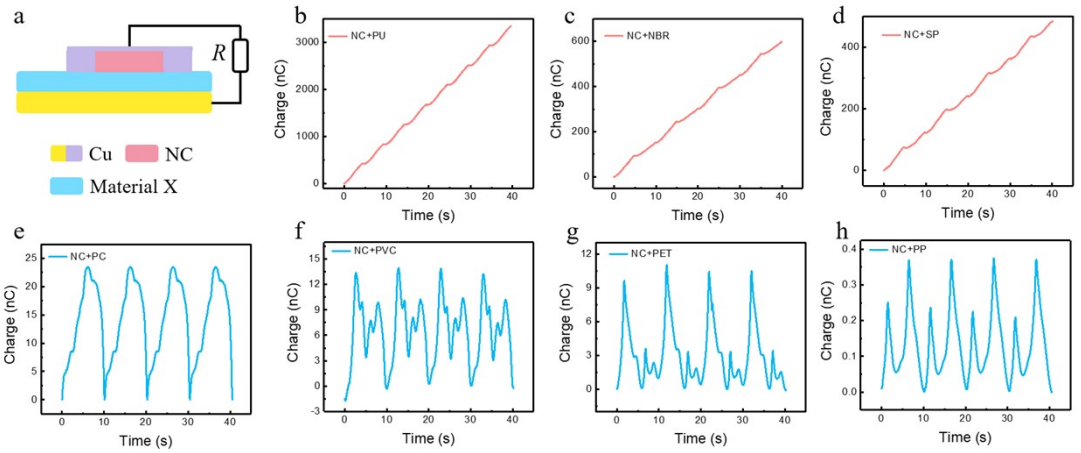

Fig. S12 Output performance of I-Q-TVNG with tribo-bias source material of NC. (a) Structure schematic of I-Q-TVNG with tribo-bias source material of NC. Output charge of I-Q-TVNG with different fixed charge deposition materials of PU (b), NBR (c), SP (d), PC (e), PVC (f), PET (g), and PP (h).

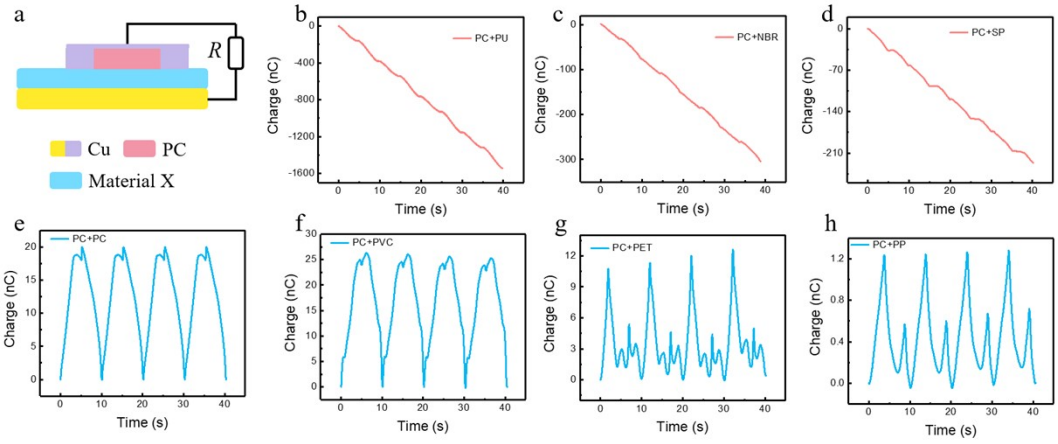

Fig. S13 Output performance of I-Q-TVNG with tribo-bias source material of PC. (a) Structure schematic of I-Q-TVNG with tribo-bias source material of PC. Output charge of I-Q-TVNG with different fixed charge deposition materials of PU (b), NBR (c), SP (d), PC (e), PVC (f), PET (g), and PP (h).

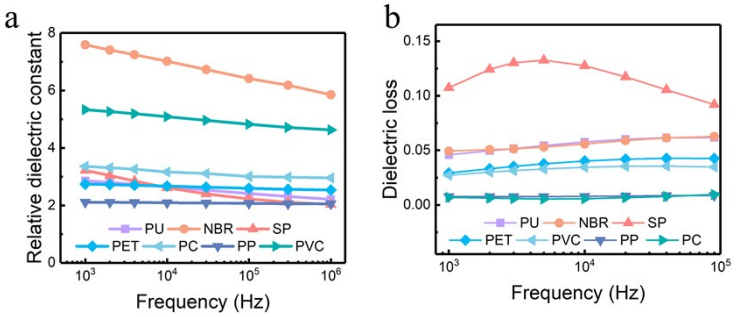

Fig. S14 Relative permittivity and dielectric loss of charge deposition materials. Relative permittivity (a) and dielectric loss (b) of the seven fixed charge deposition materials.

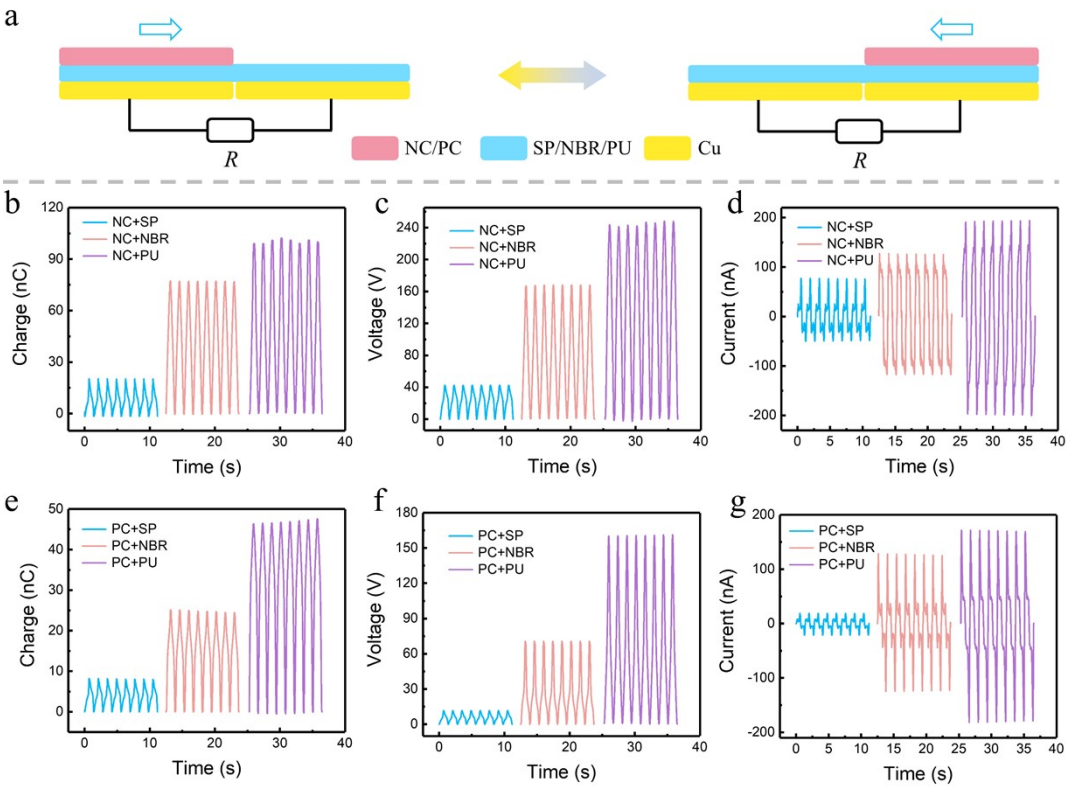

Fig. S15 Output performance of free-standing AC-TENG used to determine the triboelectric properties between different materials. (a) Schematic diagram of the free-standing TENG. Output charge (b), voltage (c), and current (d) of free-standing TENG with slider of NC and different charge deposition materials. Output charge (e), voltage (f), and current (g) of free-standing TENG with slider of PC and different charge deposition materials.

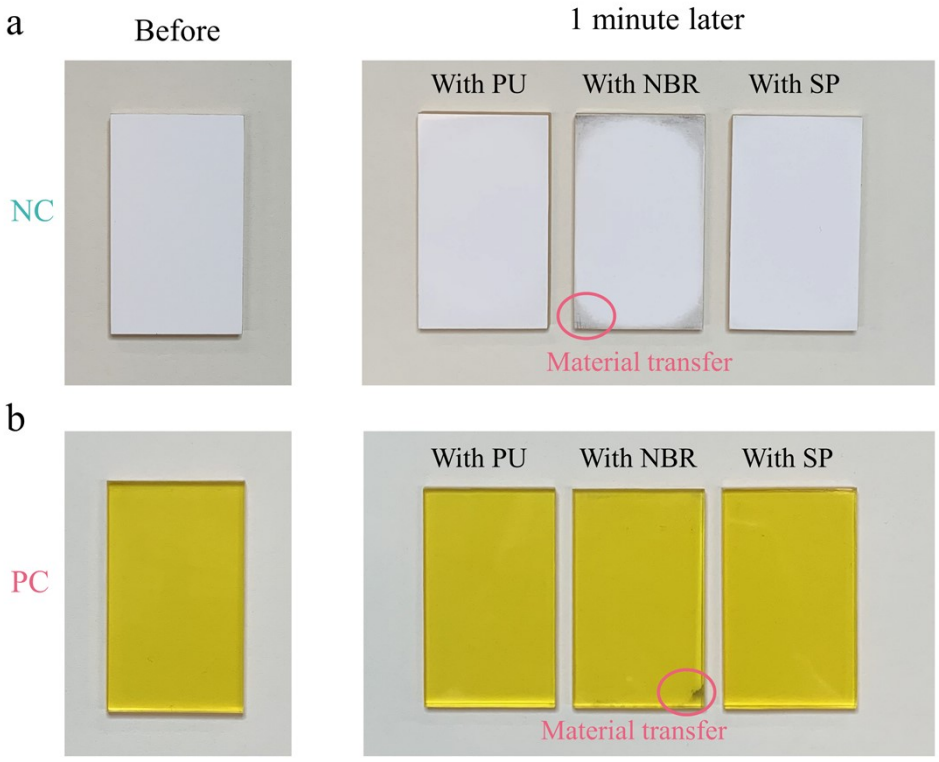

Fig. S16 Optical photographs of NC and PC. (a) Photos of NC before and after 1-minute cycle test with PU, NBR, and SP. (b) Photos of PC before and after 1-minute cycle test with PU, NBR, and SP.

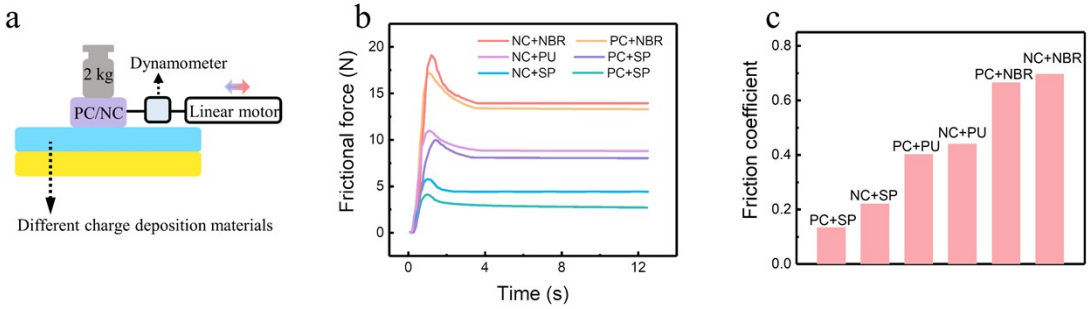

Fig. S17 Test of frictional force and friction coefficient between different friction pairs. (a) Schematic diagram of testing the frictional force of different charge deposition materials tested at a pressure of 20 N. (b) Frictional force and (c) friction coefficient between different friction pairs.

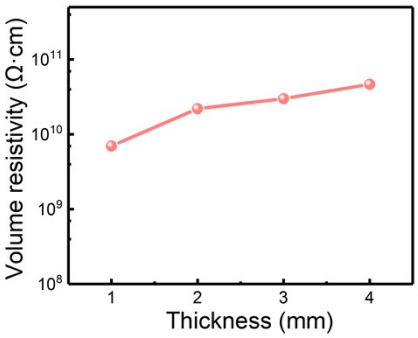

Fig. S18 Leakage current density of PU with different thicknesses.

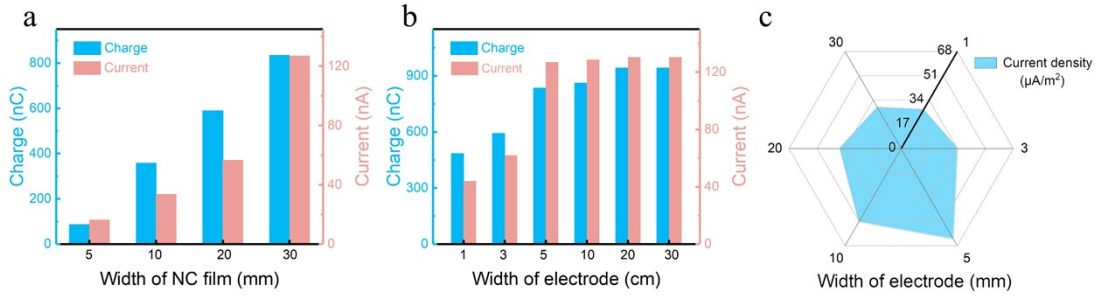

Fig. S19 Parameters affecting the output performance of I-Q-TVNG. Output performance of the device with different widths of NC film (a), and widths of top electrode (b). (c) Current density of I-Q-TVNG with different widths of top electrode.

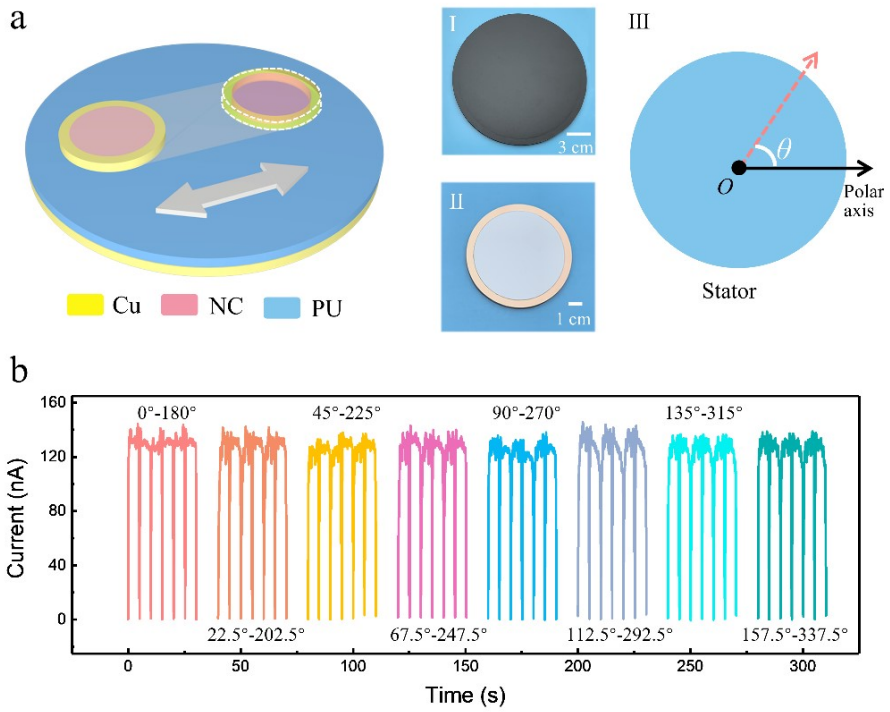

Fig. S20 Structure diagram and output current of I-Q-TVNG with a centrosymmetric slider. (a) Structure illustration of I-Q-TVNG with a centrosymmetric slider. The insert of (I) and (II) are the digital images of the stator and the slider, respectively. The insert of (III) is the defined polar coordinate system. The central position of stator is point *O* (called as pole), and the horizontal ray from this point *O* is the polar axis. The polar angle θ measures the angle from the polar axis to the sliding direction of slider (the pink dotted arrow) in a counterclockwise direction. (b) Output current of the I-Q-TVNG under different sliding directions.

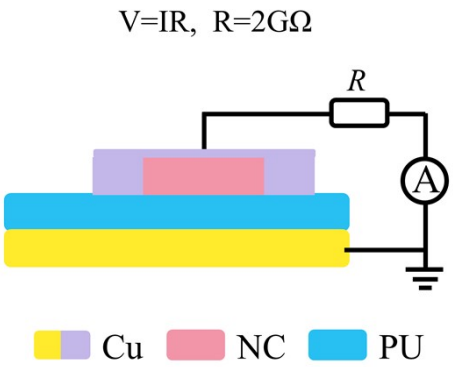

Fig. S21 Schematic diagram on measuring the voltages of the I-Q-TVNG.

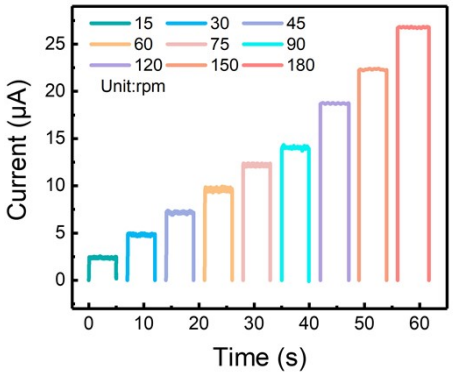

Fig. S22 Current of rotation-type I-Q-TVNG with different rotating speeds.

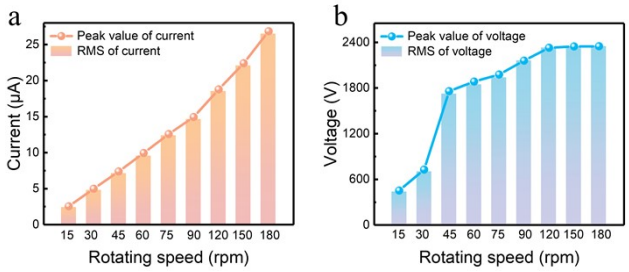

Fig. S23 Output performance of rotation-type I-Q-TVNG. (b) Peak current and RMS of steady current of I-Q-TVNG with different rotating speeds. (c) Peak voltage and RMS of steady voltage of I-Q-TVNG with different rotating speeds.

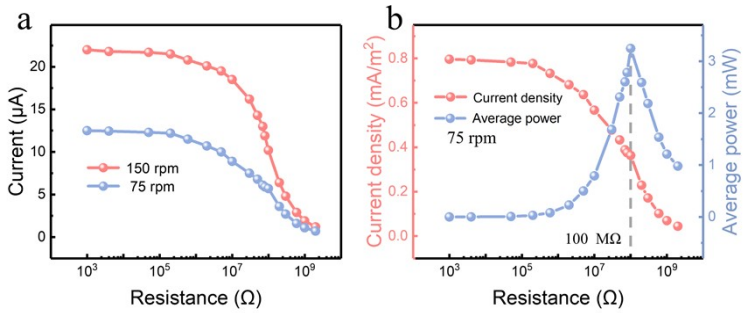

Fig. S24 Matching impendence test of I-Q-TVNG at rotating speed of 75 rpm and 150 rpm. (a) Current of the device under various external loads. (b) Current density and power at 75 rpm.

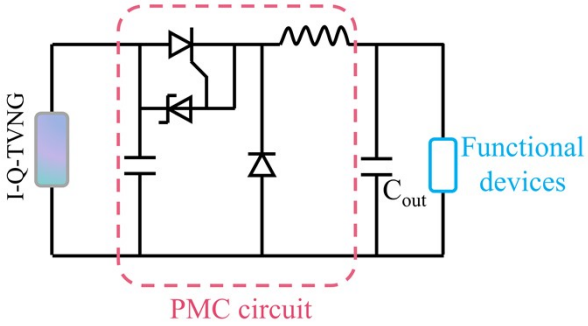

Fig. S25 Schematic diagram of PMC.

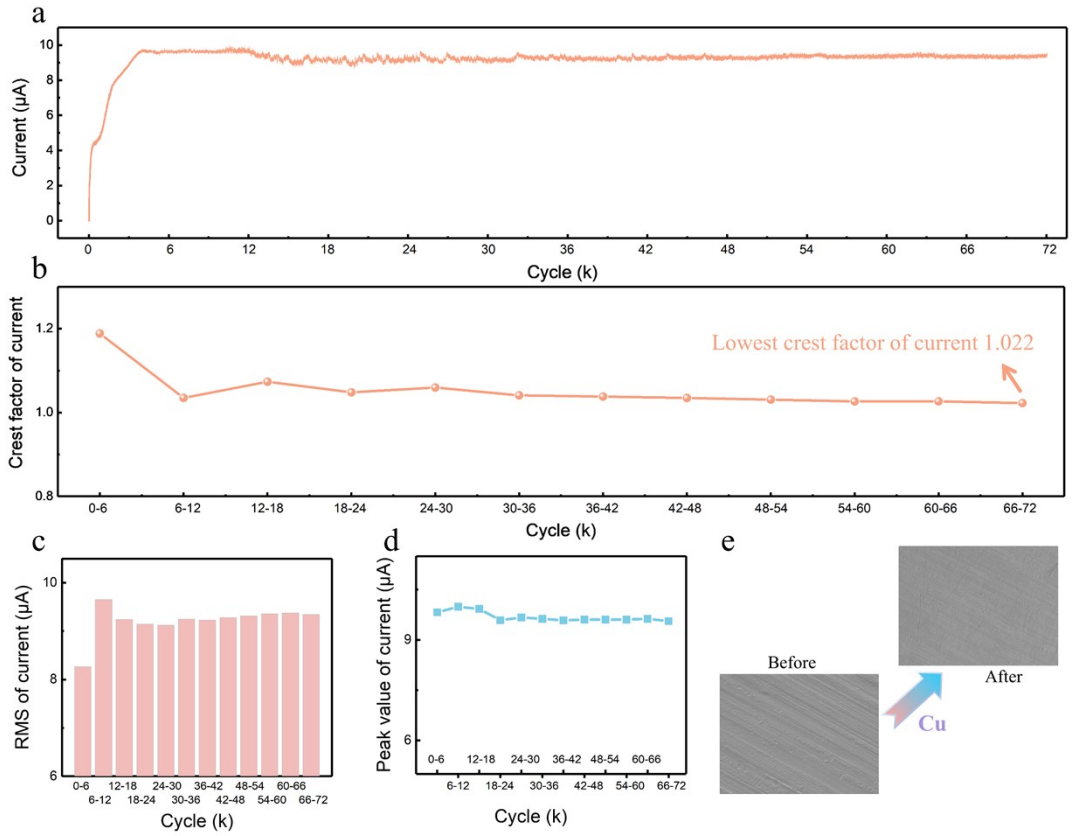

Fig. S26 Stability test of I-Q-TVNG within 72, 000 cycles. Current output (a), crest factor of current (b), peak current (c), and RMS of steady current (d) of I-Q-TVNG over 72, 000 cycles. (e) SEM images of top Cu electrode at initial and after 72, 000 cycles of continuous testing.

Supplementary Tables

Table S1. Comparison of the output voltage with the latest and most typical TVNGs based on tribovoltaic effect.[1-16]

Reference	Journals	Materials	Output voltage (V)
[1]	Advanced Energy Materials	Steel/N-Si	0.02
[2]	Advanced Energy Materials	Steel/P-Si/N-Si	0.09
[3]	Nano Micro Letter	Cu/Si/Au	0.227
[4]	Advanced Functional Materials	Cu/P-Si	0.25
[5]	Advanced Energy Materials	Conductive fabric/N-fabric	0.28
[6]	Energy Environmental Science	Al/N-Si	0.3
[7]	Nano Energy	PEDOT:PSS /Al	0.6
[8]	Advanced Functional Materials	$Pt/H_2O/IGZO$	0.62
[9]	Energy Environmental Science	Al/Polypyrrole/Au	1.06
[10]	Advanced Energy Materials	$Al/CsPbBr_3/ITO$	3.69
[11]	Journal of Materials Chemistry A	Al/PVP/Si	20
[12]	Advanced Materials	$PBi_2Te_3/NGaN$	40
[13]	Energy Environmental Science	PTFE/Nylon/Si/Cu	80
[14]	Advanced Energy Materials	Si/GaN	90
[15]	Energy Environmental Science	P-Si/N-GaN	130
[16]	Advanced Energy Materials	Steel/uGaN	130
This work		NC/PU/Cu	2324

Table S2. Comparison of the lifetime with the latest and most typical TVNGs based on tribovoltaic effect.[3, 9, 17-19]

Reference	Journals	Strategy	Cycles (k)	Output retention ratio (%)	Attenuation rate per 1 k cycles (%)
[17]	Advanced Functional Materials	Interface Lubrication	30	95	0.168
[18]	Advanced Functional Materials	Material modification	43	81.97	0.419
[19]	Advanced Materials	Material modification	20	85.29	0.736
[3]	Nano Micro Letter	Interface Lubrication	90	90	1
[9]	Energy Environmental Science	Soft contact	20	0.5 %	4.975
This work	\	Soft contact	72	97.1	0.040

References

1. Z. Zhang, D. Jiang, J. Zhao, G. Liu, T. Bu, C. Zhang and Z. L. Wang, *Adv. Energy Mater.*, 2020, **10**.
2. S. Dong, T. Bu, Z. Wang, Y. Feng, G. Liu, J. Zeng, Z. Wang, J. Cao, Z. Zhang, F. Liu and C. Zhang, *Adv. Energy Mater.*, 2023, **13**.
3. W. Qiao, L. Zhou, Z. Zhao, P. Yang, D. Liu, X. Liu, J. Liu, D. Liu, Z. L. Wang and J. Wang, *Nano-Micro Lett.*, 2023, **15**.
4. L. Gong, Z. Wang, R. Luan, G. Liu, B. Fan, Y. Feng, J. Cao, Y. Qi, Z. Zhang and C. Zhang, *Adv. Funct.Mater.*, 2023, 2310703.
5. T. Lv, R. Cheng, C. Wei, E. Su, T. Jiang, F. Sheng, X. Peng, K. Dong and Z. L. Wang, *Adv. Energy Mater.*, 2023, **13**.
6. X. Xu, Z. L. Wang and Z. Yang, *Energy Environ. Sci.*, 2024, **17**, 149-157.
7. Z. y. You, X. Wang, F. Lu, S. Wang, B. Hu, L. Li, W. Fang and Y. Liu, *Nano Energy*, 2023, **109**.
8. Y. Huang, D. Liu, X. Gao, J. Zhu, Y. Zhang and M. Zhang, *Adv. Funct. Mater.*, 2022, **33**.
9. J. Meng, C. Pan, L. Li, Z. H. Guo, F. Xu, L. Jia, Z. L. Wang and X. Pu, *Energy Environ. Sci.*, 2022, **15**, 5159-5167.
10. H. Yuan, Z. Xiao, J. Wan, Y. Xiang, G. Dai, H. Li and J. Yang, *Adv. Energy Mater.*, 2022, **12**.
11. X. Pan, H. Xiang, Z. Xuan, Y. Jie and X. Cao, *J. Mater. Chem. A*, 2023, **11**, 25377-25385.
12. Z. Zhang, Z. Wang, Y. Chen, Y. Feng, S. Dong, H. Zhou, Z. L. Wang and C. Zhang, *Adv. Mater.*, 2022, **34**.
13. C. Pan, L. N. Y. Cao, J. Meng, L. Jia, W. Hu, Z. L. Wang and X. Pu, *Energy Environ. Sci.*, 2024, 17, 1132
14. S. Qin, J. Chen, P. Yang, Z. Liu, X. Tao, X. Dong, J. Hu, X. Chu, Z. L. Wang and X. Chen, *Adv. Energy Mater.*, 2023, **14**.
15. Z. Wang, Z. Zhang, Y. Chen, L. Gong, S. Dong, H. Zhou, Y. Lin, Y. Lv, G. Liu and C. Zhang, *Energy Environ. Sci.*, 2022, **15**, 2366-2373.
16. Z. Zhang, N. Wu, L. Gong, R. Luan, J. Cao and C. Zhang, *Adv. Mater.*, 2024, 36.
17. W. Qiao, Z. Zhao, L. Zhou, D. Liu, S. Li, P. Yang, X. Li, J. Liu, J. Wang and Z. L. Wang, *Adv. Funct. Mater.*, 2022, **32**.
18. B. Fan, Z. Wang, G. Liu, Z. Wang, X. Fu, L. Gong and C. Zhang, *Adv. Funct. Mater.*, 2023, **33**.
19. F. Jiang, G. Thangavel, X. Zhou, G. Adit, H. Fu, J. Lv, L. Zhan, Y. Zhang and P. S. Lee, *Adv. Mater.*, 2023, **35**.